JOURNAL OF AIRCRAFT
Vol. 32, No. 2, March–April 1995

Wing Leading-Edge Design Concepts for Airbreathing Hypersonic Waveriders

Max L. Blosser*
NASA Langley Research Center, Hampton, Virginia 23681
Isaiah M. Blankson†
NASA Headquarters, Washington, D.C. 20546
and
Steve Schwoerke,‡ Don Brunson§, and Paul Hagseth¶
Lockheed, Fort Worth Company, Fort Worth, Texas 76101

Wing leading-edge structural concepts are considered in this article for a specific Mach 5 waverider cruise vehicle. Design tradeoffs, such as making the leading edges sharp enough for acceptable aerodynamic and propulsion efficiency, yet blunt enough for acceptable aerodynamic heating, are discussed. Aerodynamic heating distributions are calculated for two locations on the leading edge of the vehicle. Several structural concepts are discussed and a particular concept is studied. Temperature and thermal stress distributions are calculated for a simple wing leading-edge concept consisting of an uninsulated hot structure. Techniques for reducing thermal stresses are discussed.

Introduction

WORLD-WIDE interest in hypersonic flight has recently been renewed. A wide range of vehicle concepts—cruise, single-stage-to-orbit (SSTO) and two-stage-to-orbit (TSTO) vehicles—are being considered. Waveriders are one class of hypersonic vehicle under consideration.

A waverider (originally proposed in Ref. 1) is a supersonic or hypersonic vehicle that has an attached shock along its leading edge. The vehicle appears to be riding on top of its shock wave—hence the name "waverider." Because the shock is attached to the leading edge of the vehicle, the upper and lower surfaces of the vehicle can be designed separately. In addition, this attached shock prevents spillage of higher pressure air from the lower side of the vehicle to the upper side, thus resulting in a vehicle with potential for a high lift-to-drag ratio.

For Mach 4-7 flight, waverider vehicles are under consideration as candidates for short- and long-range cruise missions.[2–4] Although the waverider is usually regarded as a cruise vehicle, several ongoing studies[5,6] have shown that it is also a suitable configuration for TSTO and SSTO applications. In particular, for the mission studied in Ref. 5, a waverider vehicle clearly outperformed a lifting body vehicle. Excellent and authoritative surveys of waverider research have been given by Townend,[7] Roe,[8] and Schindel.[9]

Waverider principles were used in the design of the half-million-lb XB-70 Valkyrie supersonic bomber. This aircraft achieved an L/D of about 7 at Mach 3 in test flights in the mid-1960s. The XB-70 program demonstrated the high L/D potential and the practical applicability of waverider concepts to full-scale cruise aircraft.

One of the key issues concerning waveriders is the design of the wing leading edges. Current techniques for designing waverider shapes assume infinitely sharp wing leading edges. Sharp leading edges are also desirable for efficient propulsion, because the forebody of the vehicle is used to compress the air flowing into the engines. Blunt leading edges can result in thick boundary layers being ingested into the engines, thereby degrading the propulsion efficiency. However, because the heating rate to the leading edge is a strong function of the leading-edge radius, the leading edge must be blunted to reduce heating rates to acceptable levels. This blunting of the leading edge can change the planform shape of the vehicle. Also, the aerodynamic performance of the vehicle may be degraded because the shock is detached from the blunted leading edges, thereby allowing high-pressure air to spill from the lower surface of the vehicle to the upper surface. Studies by Squire[10,11] showed that, for delta wings, appreciable shock standoff distances did not result in significant spillage. Leading-edge bluntness effects on caret wings were considered by Collingbourne and Peckham.[12] Estimates were made of the simultaneous decrease in lift and increase in drag for given nose bluntness. Their conclusions emphasize the importance of designing for the smallest possible leading-edge radii. He and Rasmussen[13] showed that rounding the leading edges of a Mach 8.3 waverider to 96% of the span resulted in a 3% loss of L/D. Losses at off-design Mach numbers were shown to be less than 3%. Thus, designing a waverider leading edge involves a tradeoff between making the leading edge sharp enough to obtain acceptable aerodynamic and propulsion efficiency, yet blunt enough to use a reliable, efficient structural configuration.

In this article, wing leading-edge concepts are proposed for a particular Mach 5 waverider vehicle.[14] The Mach 5 waverider is briefly described, and aerodynamic heating rate distributions are calculated for two locations on the leading edge of the vehicle. Several leading-edge structural concepts are described, and one concept is analyzed in detail to predict its

Presented as Paper 94-0379 at the AIAA 32nd Aerospace Sciences Meeting and Exhibit, Reno, NV, Jan. 10–13, 1994; received Feb. 14, 1994; revision received June 7, 1994; accepted for publication June 14, 1994. Copyright © 1994 by the American Institute of Aeronautics and Astronautics, Inc. No copyright is asserted in the United States under Title 17, U.S. Code. The U.S. Government has a royalty-free license to exercise all rights under the copyright claimed herein for Governmental purposes. All other rights are reserved by the copyright owner.

*Aerospace Engineer, Thermal Structures Branch, M/S 396.
†Deputy Director, Hypersonics Research Division, Code RN. Senior Member AIAA.
‡Engineering Specialist, Flight Sciences, MZ 4207.
§Engineering Specialist, Flight Sciences, MZ 2892.
¶Senior Engineering Specialist, Flight Sciences, MZ 4207. Member AIAA.

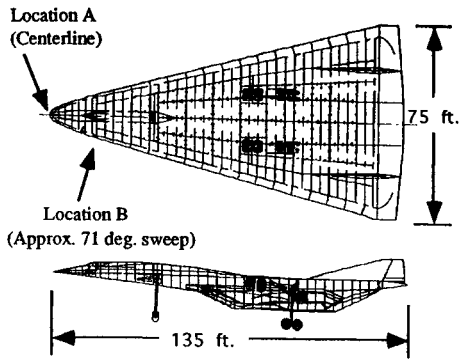

Fig. 1 Top and side views of Mach 5 waverider.

thermal and mechanical response to the incident aerodynamic heating.

Vehicle Description

A Mach 5 waverider aircraft (Fig. 1) was developed and analyzed[14] in an attempt to better quantify the characteristics of such a vehicle and assess its potential. The mission goals for this vehicle included a 6000 n.mi. range, 350,000 lb weight class, 5000-lb payload, and endothermic fuel. The vehicle was derived from a conical waverider to take advantage of the computationally simple inverse design methods developed for generating waverider shapes.

A conical-flow waverider with an approximately 8-deg cone angle was chosen as the best L/D design, based on previous parametric waverider design studies. An aerodynamically optimized, pure waverider shape typically has high anhedral drooping wings, which can provide poor structural load paths, potential ground clearance problems at takeoff, and unknown lateral-directional stability effects at hypersonic speeds. The shape selected for this vehicle sacrificed some L/D performance to achieve a better integrated design. The aft lower fuselage was modified to accommodate the four turboramjet engine modules and the engine nozzle. The base was tapered to a sharp wing trailing edge, and vertical fins and a cockpit were added to the upper surface. The result was a flat upper surface, a semiconical lower surface, and a fairly conventional lower compression surface and engine integration configuration.

A fairly comprehensive assessment of the vehicle is described in Ref. 14, including propulsion system design, thermal management assessment, system integration, and structural design and analysis. A particularly critical aspect of the vehicle design that requires further investigation is the leading edge of the waverider forebody. A leading-edge radius of 0.25 in. was chosen for this study as an initial estimate to provide a leading edge with good aerodynamic performance, yet acceptable heating rates. The remainder of this article addresses the feasibility of developing a simple structural concept for a wing leading edge with this radius.

Leading-Edge Heating

The most critical design loading for the leading edge is aerodynamic heating. Heat flux distributions about the leading edge were calculated for steady-state cruise conditions at Mach 5, with a dynamic pressure of 655 psf, laminar flow, and a 5.27-deg angle of attack.

Heat flux distributions were calculated for two locations on the vehicle: 1) along the centerline of the vehicle (location A in Fig. 1) and 2) normal to the leading edge (location B in Fig. 1). The distributions were calculated over the first 4 ft of the upper and lower surfaces at these locations assuming a leading-edge radius of 0.25 in.

Three methods were used to calculate heat fluxes for the leading edge. A computational fluid dynamics (CFD) computer code called the nose solution code (NSC) was used to analyze a two-dimensional slice of the vehicle centerline at location A in Fig. 1. NSC, developed at Lockheed Fort Worth Company and used extensively for blunt body analysis of the National Aerospace Plane, is a computer code that approximately solves the Navier-Stokes equations that govern fluid flow. A second computer code, Aeroheat, was used to predict the heat flux distributions at both the centerline and the swept leading edge. Aeroheat is a modification of the Aerhet[15] code. It uses an integral technique to relate the change of momentum thickness to the edge condition, streamline spreading rate, and skin friction. Surface streamlines are traced to determine the spreading rate. The edge conditions come from impact pressure laws for pressure and an entropy swallowing technique for entropy. Empirical relations are used to relate momentum thickness to skin friction, and skin friction is converted to heat transfer through Reynolds analogy. However, accuracy of the method near sharp leading edges is limited because of difficulties in getting a sufficient number of streamlines near the stagnation point. For improved accuracy, Fay-Riddell theory[16] was used to calculate stagnation point heat fluxes for both the centerline and swept locations.

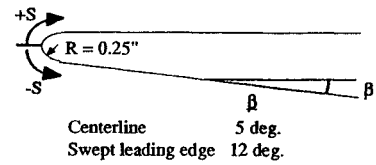

Fig. 2 Geometry for heating calculations.

The two-dimensional slices of the vehicle geometry, for which the heat flux distributions were calculated, are illustrated in Fig. 2. For both the vehicle centerline and the swept leading edge, the geometry is approximately represented by a wedge with a flat top and a 0.25-in.-radius leading edge—although the actual lower surface of the vehicle in these locations is slightly curved. The wedge angle for the centerline is approximately 5 deg, and the wedge angle of the swept leading edge is approximately 12 deg. For the purposes of this study, the canopy on the centerline of the vehicle was neglected. The origin of the surface coordinate S is located at the vertical tangent point of the leading edge. Surface coordinates are positive in the direction of the upper surface and negative in the direction of the lower surface as shown in Fig. 2.

Calculated heat flux distributions for the vehicle centerline are shown in Fig. 3a. As expected, the heat fluxes are significantly higher in the vicinity of the leading edge and drop off sharply a short distance away from the leading edge. The heat flux distribution at the leading edge is shown in more detail in Fig. 3b. The CFD analysis and the Fay-Riddell predictions agree almost exactly. Although the less accurate code, Aeroheat, predicts nearly the same heat flux near the stagnation point, it predicts significantly lower heat fluxes where the curved leading edge joins the flat forebody structure. This discrepancy occurs primarily because the pressures calculated using the impact pressure method in Aeroheat are underpredicted in this region. Away from the leading edge ($-10 < S < 10$), the CFD and Aeroheat codes show good agreement.

The calculated heating rate distributions for the swept leading edge (location B in Fig. 1) are shown in Figs. 3a and 3b. Heat fluxes, calculated using the Aeroheat code, are significantly lower at the stagnation point than the heat flux calculated using the Fay-Riddell method. The more accurate CFD calculations were not available for the swept leading-edge case, and so the Aeroheat results were adjusted to produce a distribution similar to the CFD results in Figs. 3a and 3b. The resulting faired heat flux distribution, shown in Figs. 4a and 4b was used as the thermal loading for the thermal analysis of the swept leading edge.

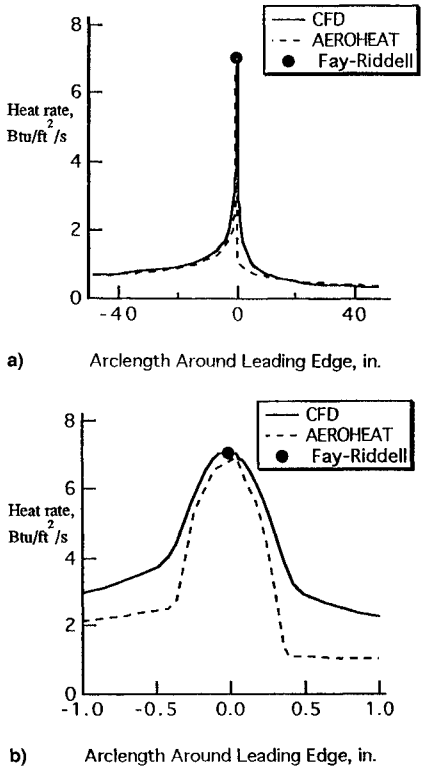

Fig. 3 a) Heat flux distribution around centerline leading edge and b) a magnified view.

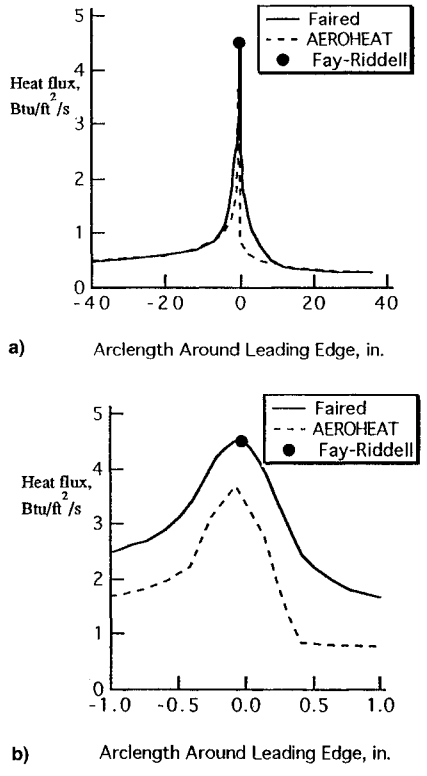

Fig. 4 a) Heat flux distribution around swept leading edge and b) a magnified view.

Leading-Edge Structural Concepts

A variety of structural concepts have been proposed for wing leading edges of hypersonic vehicles. Several concepts investigated for the National Aero-Space Plane are described in Refs. 17 and 18. Possible concepts include structures that are insulated, hot, convectively cooled, and transpiration cooled

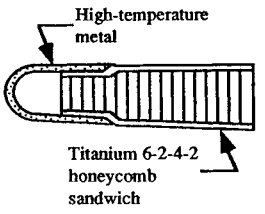

Fig. 5 Leading-edge structural configuration—concept 1.

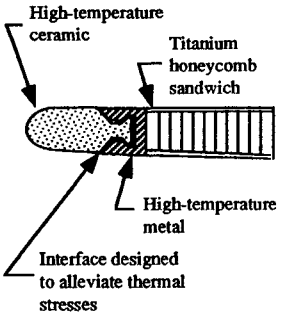

Fig. 6 Leading-edge structural configuration—concept 2.

(e.g., Ref. 19). Other concepts include ablation, heat absorbing structures, heat pipes,[20] and highly conductive materials.[21]

The leading edges for the Mach 5 waverider of the present study must maintain the geometry illustrated in Fig. 2 while subjected to a mild aerodynamic pressure load and the heat fluxes shown in Figs. 3 and 4. Insulated systems are not attractive candidates because there is so little thickness available for insulation and most insulating materials would not result in a durable leading edge. Ablators can be ruled out because of the need to maintain the leading-edge geometry. The calculated maximum stagnation heat fluxes are not high enough to require a complicated active cooling or heat pipe system. Therefore, the leading edges considered in this study are hot structures.

A simple leading-edge concept is shown in Fig. 5. The concept consists of full-depth titanium honeycomb sandwich with an overlapping leading-edge shell made of a higher temperature metal. Incoloy 909 was chosen for evaluation in the present study as the material for the high-temperature leading edge. The leading-edge material may be firmly attached to the titanium sandwich so that no slippage may occur, or it may be segmented along the leading edge with all fasteners but one on each segment to have oversized or slotted holes to allow differential thermal expansion to occur. The full-depth honeycomb sandwich may be firmly attached to the adjacent wing structure (not shown in Fig. 5), or the attachment may allow for differential thermal expansion between the honeycomb sandwich and the adjacent wing structure.

A leading-edge structural concept that may be useful for sharper radii and/or higher Mach numbers is shown in Fig. 6. The leading edge is a solid piece of high-temperature ceramic material (e.g., hafnium diboride, carbon-silicon carbide, etc.), attached to a high-temperature metal (e.g., Incoloy 909), which is then attached to a titanium honeycomb sandwich. The thermal expansion mismatch between the ceramic and the high-temperature metal can be significantly reduced by shaping the interface between these two materials using the thermal-stress alleviation principles of Ref. 22, as shown in Fig. 6. To further reduce thermal stresses, the ceramic leading edge could be segmented and each segment prevented from sliding along the leading edge by a retaining pin of high-temperature metal.

Although both leading-edge structural concepts are potentially feasible, the simpler of the two, concept 1, was selected for further analysis in this article.

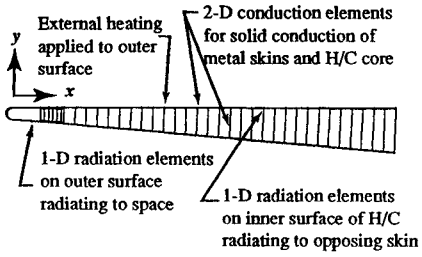

Fig. 7 Leading-edge thermal model.

Thermal Analysis

To calculate the structural response of the leading edge to the aerodynamic heating it is first necessary to calculate the resulting temperature distribution. Because the leading-edge structural concepts are thin and directly exposed to the aerodynamic heating, the leading-edge temperatures will closely follow the heating with little thermal lag. Therefore, a steady-state thermal analysis should be sufficient to accurately predict temperatures during cruise conditions.

A two-dimensional finite element model was constructed of the geometry illustrated in Fig. 5. The thermal analysis processors of the engineering analysis language[23] (EAL), version 3.30, were used to calculate temperatures.

The finite element thermal model is shown in Fig. 7. The model represents a two-dimensional slice normal to the leading edge. Two-dimensional conduction elements were used to model heat conduction in the titanium honeycomb face sheets and the Incoloy 909 leading-edge material. A single element was used in the thickness direction of the honeycomb skins and two elements in the thickness direction of the leading edge material. Material properties for Incoloy 909 and titanium 6-2-4-2 were obtained from Ref. 24. One-dimensional radiation elements on the outer surface were used to model radiation to space assuming an emissivity of 0.8. External heat flux distributions shown in Figs. 3 and 4 were applied to the outer surface. Radiation from the inner surface of the Incoloy 909 leading edge was neglected for simplicity (equivalent to assuming the interior cavity is filled with an opaque, perfect insulator). Perfect thermal contact is assumed between the leading-edge material and the honeycomb face sheets where they overlap. Heat transfer through the honeycomb core was modeled using the method proposed by Swann and Pitman.[25] One-dimensional radiation elements were used to model the radiation exchange between the inner surfaces of the honeycomb face sheets through the core. Effective radiation view factors proposed in Ref. 25 were used. Two-dimensional conduction elements, using effective conductivities calculated by the method of Ref. 25, were used to model the thermal conduction through the honeycomb core.

The particular dimensions were chosen somewhat arbitrarily in an attempt to obtain a representative geometry for analysis. The total model is approximately 14 in. long. The leading-edge radius is 0.25 in. The Incoloy 909 leading edge is 0.05 in. thick, and the honeycomb face sheets are 0.04 in. thick. The honeycomb core cell size is 0.375 in., and the cell wall thickness is 0.004 in. The leading-edge material overlaps the honeycomb by 0.75 in.

The calculated temperature distribution along the outer surface of the vehicle centerline (location A on Fig. 1) is shown in Fig. 8. The dashed line on the figure represents the radiation equilibrium temperature distribution, assuming an emissivity of 0.8. The radiation equilibrium temperature is calculated assuming that all incident heat is reradiated (i.e., the surface is perfectly insulated). The maximum calculated radiation equilibrium temperature is 1616°F. However, thermal conduction in the leading edge reduces the predicted maximum temperature to 1400°F, which is within the acceptable temperature range for Incoloy 909. As expected, the

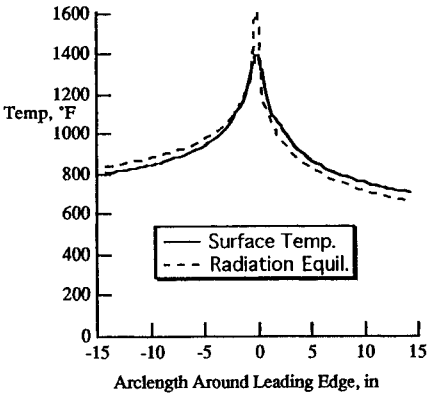

Fig. 8 Leading-edge centerline temperature distributions.

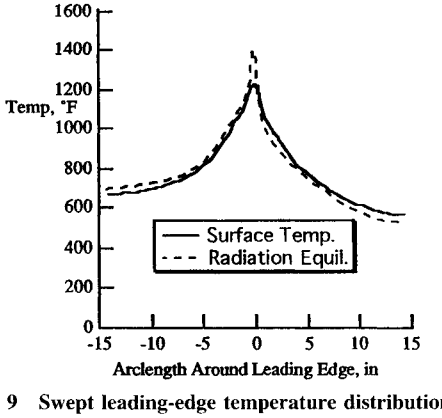

Fig. 9 Swept leading-edge temperature distributions.

temperature peaks at the stagnation point and drops off sharply away from the leading edge. The predicted temperature aft of the nose region on the upper surface is higher than the radiation equilibrium temperature, and the temperature on the lower surface is lower than radiation equilibrium. These differences between the predicted temperatures and radiation equilibrium temperatures are an indication of the heat transfer occurring from the lower surface through the honeycomb core to the upper surface. The temperature variations through the thicknesses of the leading-edge shell and the honeycomb face sheets were found to be negligible.

The calculated temperature distribution along the outer surface of the swept leading edge (location B on Fig. 1) is shown in Fig. 9. The dashed line on the figure represents the radiation equilibrium temperature distribution, assuming an emissivity of 0.8. The maximum calculated radiation equilibrium temperature is 1396°F. However, thermal conduction in the leading edge reduces the predicted maximum temperature to 1227°F. Again, this temperature is well within the acceptable temperature range for Incoloy 909. The shape of the temperature distribution for the swept leading edge is very similar to that shown in Fig. 8 for the centerline case.

Structural Analysis

Although the temperatures shown in Figs. 8 and 9 are within the acceptable range for the materials being used, structural analysis is required to determine if thermal stresses are acceptable. Stresses resulting from aerodynamic pressure loading were assumed to be secondary to the thermal stresses, and were therefore ignored.

Both the leading-edge geometry and heating distributions vary gradually along the leading edge, but sharply normal to it. Therefore, for simplicity, the equivalent to a generalized plane strain analysis was used to calculate the thermal stresses of the leading edge. However, if the leading edge is segmented

along the leading edge with gaps between segments, there is a traction-free surface at the end of each segment where the plane strain analysis is not valid. Near the ends of the segments, the thermal stresses will be significantly lower than those predicted using the plane strain analysis, so that providing many short segments along the leading edge may reduce the thermal stresses even below the magnitudes of thermal stress predicted in this article.

The structural analysis was completed using the structural processors of EAL.[23] A single layer of three-dimensional elements along the leading edge was used to calculate the thermal stresses. These three-dimensional elements were required to impose the out-of-plane boundary conditions. The same in-plane nodal locations were used as for the thermal model shown in Fig. 7. A duplicate set of nodes offset by 0.2 in. along the leading edge (z direction) was used to define the three-dimensional elements used in the structural model. In the areas where the Incoloy 909 skin overlaps the titanium honeycomb sandwich, one-dimensional, zero-length elements with stiffness defined only normal to the surfaces of the sheets were used to model the joint. This finite element modeling strategy was used to represent fasteners with slotted or oversized holes to allow differential thermal expansion tangential to the joint. Equations from Ref. 26 were used to calculate a consistent set of elastic stiffness properties for the honeycomb core. The temperatures calculated in the thermal analysis for each node were transferred to the structural model to provide the thermal loading. The structure was assumed to be free of thermal stresses at 70°F.

Three different boundary conditions were investigated. For all three boundary conditions, the nodes on the end of the model away from the leading edge were prevented from moving in the x direction, and a single node on the lower surface was prevented from moving in the y direction (to prevent rigid body motion). The z displacements prescribed in the different boundary conditions are shown in Fig. 10. Along the plane of $z = 0$, all of the nodes were prevented from moving in the z direction. For the nodes on the $z = 0.2$ in. plane, results were calculated for three different imposed displacements in the z direction. For boundary condition 1 ($\delta_1 = \delta_2 = 0$) all of the nodes on the $z = 0.2$ in. plane were fully constrained in the z direction. This condition prevents thermal growth in the z direction. For boundary condition 2 ($\delta_1 = \delta_2$), all of the nodes on the $z = 0.2$ in. plane were given a uniform displacement, the magnitude of which was determined iteratively, such that the sum of the reactions in the z direction was zero. This is equivalent to tying the Incoloy 909 leading edge and the full-depth titanium honeycomb sandwich together, but allowing this combination to freely expand while preventing bending about the x or y axes. The third boundary condition ($\delta_1 \neq \delta_2$) applies different z displacements to the Incoloy 909 and the titanium honeycomb sandwich, so that each of them individually has zero net reactions in the z direction. Both the Incoloy 909 and the titanium honeycomb sandwich are allowed to expand freely in the z direction, but not to bend about the x or y axes.

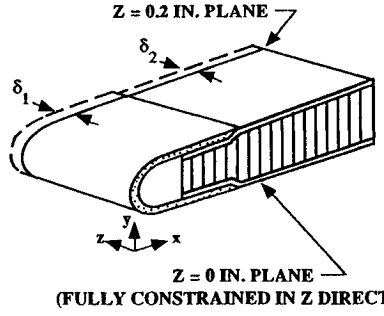

Fig. 10 Applied displacements in z direction.

The stresses in the z direction were found to be the predominate thermal stresses. All of the in-plane stresses were below 1000 psi. Variations of z stresses through the thickness of the Incoloy 909 and the titanium face sheets were found to be insignificant.

The thermal stresses in the z direction for the centerline leading edge are shown for the three constraint cases in Fig. 11. The "v-shaped" portion of the curve represents the thermal stresses in the z direction on the Incoloy 909 leading edge. The curves to the left and to the right on each figure represent thermal stresses in the lower and upper face sheets, respectively, of the titanium honeycomb sandwich. The maximum compressive stress in the Incoloy 909 leading edge is −153,000 psi for the fully constrained boundary condition. The yield stress for Incoloy 909 at 1400°F is approximately 80,000 psi, and so the stresses for the fully constrained condition would be beyond yield. For boundary condition 2, some thermal expansion is allowed to occur and the maximum compressive stress drops to −46,000 psi, which is below the yield stress. For boundary condition 3, additional thermal expansion is allowed to occur and the maximum thermal stress is reduced to −23,000 psi. For all three boundary conditions the stress distributions have the same characteristic shapes. These shapes are directly related to the temperature distributions. The stresses can be greatly reduced by incorporating some means to allow thermal expansion to occur, as illustrated by boundary conditions 2 and 3.

The thermal stresses for the swept leading edge are shown in Fig. 12. The stress distributions are similar to those for the centerline case, with slightly lower stress levels. For boundary condition 1, the maximum compressive stress is −133,000 psi, which slightly exceeds the yield stress of Incoloy 909 at 1200°F (−125,000 psi). The maximum compressive stress for boundary condition 2 is −41,000 psi, and for boundary condition 3 the maximum stress is −16,000 psi. These calculations show

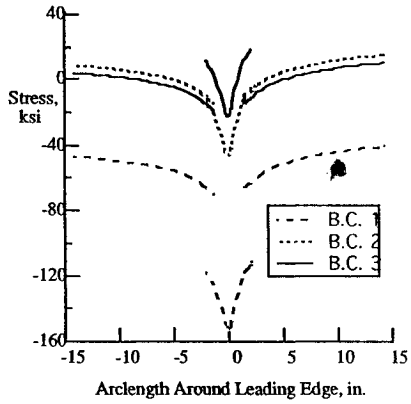

Fig. 11 Thermal stress distribution for centerline leading edge.

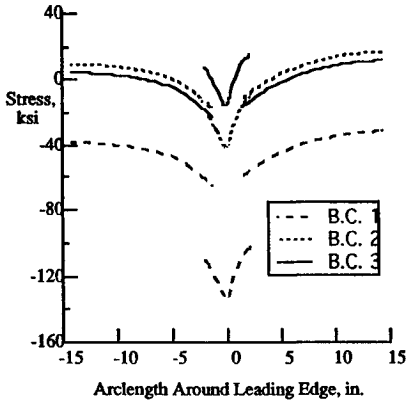

Fig. 12 Thermal stress distribution for swept leading edge.

that the thermal stresses can be reduced to acceptable levels by designing the components of the leading-edge configuration to allow some thermal expansion.

Concluding Remarks

The research and technology needs for addressing the wing leading-edge design of hypersonic waverider vehicles are examined. Leading-edge heating protection of waveriders is a key technology. The leading-edge design for a particular Mach 5 waverider vehicle was addressed. Aerodynamic heating rate distributions were calculated for two locations on the leading edge of the vehicle. Several possible leading-edge structural concepts were discussed and one concept was studied in detail. The leading-edge concept studied consisted of a thin shell of Incoloy 909 attached to a full-depth honeycomb sandwich made of titanium 6-2-4-2. A two-dimensional thermal and structural finite element analysis was used to calculate the temperature distributions and associated thermal stress distributions for this concept. Temperatures were found to be well within the acceptable limits of the materials used. Thermal stresses were found to be significant, but techniques for reducing the thermal stresses to within acceptable limits were discussed. Based on the results of this study, a simple, passive, uninsulated leading-edge structure appears attractive for the Mach 5 waverider vehicle studied.

References

[1]Nonweiler, T. R. F., "Aerodynamic Problems of Manned Space Vehicles," *Journal of the Royal Aeronautical Society*, Vol. 63, 1959, pp. 521–528.

[2]Blankson, I. M., "Prospects for Air-Breathing Hypersonic Waveriders," AIAA Paper 92-0303, Jan. 1992.

[3]Hagseth, P., and Blankson, I. M., "Current Technologies for Waverider Aircraft," AIAA Paper 93-0400, Jan. 1993.

[4]Blankson, I. M., and Hagseth, P., "Propulsion Airframe Integration Issues for Waveriders," AIAA Paper 93-0506, Jan. 1993.

[5]Kossira, H., and Heinze, W., "Investigations on the Potential of Hypersonic Waveriders with the Integrated Aircraft Design Program PrADO-Hy," AIAA Paper 93-5098, Nov.–Dec. 1993.

[6]Molvik, G. A., Bowles, J. V., and Huynh, L. C., "Analysis of a Hypersonic Research Vehicle with a Hydrocarbon Scramjet Engine," AIAA Paper 93-0509, Jan. 1993.

[7]Townend, L. H., "Research and Design for Lifting Reentry," *Progress in Aerospace Sciences*, Vol. 19, No. 1, 1979, pp. 1–80.

[8]Roe, P. L., "Theory of Waveriders," *Aerodynamic Problems of Hypersonic Vehicles*, edited by K. Enkenhus, J. F. Wendt, and R. C. Pankhurst, AGARD LS-42, 1972.

[9]Schindel, L. H., "Tactical Missile Aerodynamics," edited by M. S. Hemsch and J. N. Nielsen, Vol. 104, Progress in Astronautics and Aeronautics, AIAA, New York, 1986.

[10]Squire, L. C., "The Independence of Upper and Lower Wing Flows at Supersonic Speeds," *The Aeronautical Journal*, Vol. 80, Oct. 1976, pp. 452–456.

[11]Squire, L. C., "Flow Regimes over Delta Wings at Supersonic and Hypersonic Speeds," *Aeronautical Quarterly*, Vol. 27, Feb. 1976, pp. 1–14.

[12]Collingbourne, J. R., and Peckham, D. H., "The Lift and Drag Characteristics of Caret Wings at Mach Numbers Between 5 and 10," Ames Research Center, ARC CP 930, Feb. 1966.

[13]He, X., and Rasmussen, M. L., "Computational Analysis of Off-Design Waveriders," AIAA Paper 93-3488, Aug. 1993.

[14]Pegg, R. T., et al., "Design of a Hypersonic Waverider-Derived Airplane," AIAA Paper 93-0401, Jan. 1993.

[15]Fivel, H. J., "Numerical Flowfield Program for Aerodynamic Heating Analysis, User's Manual," Air Force Wright Aeronautical Labs., AFWAL-TR-85-3054, Aug. 1985.

[16]Fay, J. A., and Riddell, F. R., "Theory of Stagnation Point Heat Transfer in Dissociated Air," *Journal of Aeronautical Sciences*, Vol. 25, No. 2, 1958, pp. 54–67.

[17]Camarda, C. J., and McGowan, D. M., "Leading Edges for NASP—A Status Report," NASP TM 1022, June 1988.

[18]Camarda, C. J., "Results of Generic Studies of Leading Edges," 10th National Aero-Space Plane Symposium, Paper 155, Monterey, CA, April 1991.

[19]Hebrard, P., Gay, H., and Le Touche, R., "Metallic Leading Edge with Active Thermal Protection," 41st Congress of the International Astronautical Federation, IAF Paper 90-284, Dresden, Germany, Oct. 1990.

[20]Glass, D. E., and Camarda, C. J., "Preliminary Thermal/Structural Analysis of a Carbon-Carbon/Refractory-Metal Heat-Pipe-Cooled Wing Leading Edge," *Thermal Structures and Materials for High-Speed Flight*, edited by E. A. Thornton, Vol. 140, Progress in Astronautics and Aeronautics, AIAA, Washington, DC, 1992.

[21]Nonweiler, T. R. F., "The Waverider Wing in Retrospect and Prospect: A Personalized View," *Proceedings of the 1st International Waverider Symposium*, Univ. of Maryland, College Park, MD, 1990, pp. 1–24.

[22]Blosser, M. L., "Thermal-Stress-Free Fasteners for Joining Orthotropic Materials," *AIAA Journal*, Vol. 27, No. 4, 1989, pp. 472–478.

[23]Whetstone, W. D., "EISI-EAL Engineering Analysis Language Reference Manual, System Level 312," Engineering Information Services, Inc., San Jose, CA, Aug. 1985.

[24]Anon., *Aerospace Structural Metals Handbook*, CINDAS/USAF Handbooks Operation, Purdue Univ., West Lafayette, IN, 1993.

[25]Swann, R. T., and Pittman, C. M., "Analysis of Effective Thermal Conductivities of Honeycomb-Core and Corrugated-Core Sandwich Panels," NASA TN D-714, April 1961.

[26]Gibson, L. J., and Ashby, M. F., *Cellular Solids, Structure and Properties*, Pergamon, Oxford, England, UK, 1988.